Open access • Journal Article • DOI:10.1039/C3DT51100F

Solvent dependent anion dissociation limits copper(I) catalysed atom transfer reactions — Source link

Timothy J. Zerk, Paul V. Bernhardt

Institutions: University of Queensland

Published on: 23 Jul 2013 - Dalton Transactions (The Royal Society of Chemistry)

Topics: Atom-transfer radical-polymerization, Catalysis, Denticity, Dissociation (chemistry) and Oxidation state

Solvent dependent anion dissociation limits copper(I) catalysed atom transfer reactions

Timothy J. Zerk and Paul V. Bernhardt*

School of Chemistry and Molecular Biosciences, University of Queensland, Brisbane 4072, Australia

Email: p.bernhardt@uq.edu.au

Abstract

Atom transfer radical addition (ATRA) and polymerization (ATRP) reactions are commonly catalyzed by copper(I) complexes which react, reversibly, with a dormant alkyl halide initiator (RX) releasing a reactive organic radical R$^{\cdot}$. The copper catalyst bears a multidentate N-donor ligand (L) and the active catalyst is simply $Cu^{I}L$. The role of the catalyst in these reactions is to abstract a halogen atom from RX forming the corresponding higher oxidation state species $Cu^{II}LX$. However, in order to perform its catalytic function (in multiple turnovers) the halido ligand must be released from the copper ion *en route* to regenerating the active catalyst $Cu^{I}L$. In this work we investigate the kinetics of the $Cu^{I}LX/Cu^{I}L$ equilibrium where L is the tridentate *N,N,N′,N″,N″*-pentamethyldiethylenetriamine (PMDETA). Using electrochemical analysis we discovered that the rate of formation of the active catalyst $Cu^{I}L$ is strongly dependent on solvent. We demonstrate that both the kinetics and thermodynamics of this simple ligand exchange reaction are critical in the overall reaction pathway.

1. Introduction

As one of the most important forms of controlled reversible-deactivation radical polymerization[1] (traditionally known as living/controlled radical polymerization), atom transfer radical polymerization (ATRP)[2, 3] is capable of producing a vast array of polymers with well-defined compositions, architectures and functionalities.[4] This reaction is commonly catalysed by a transition metal complex stable in two different oxidation states; most commonly a Cu(II/I) complex.

Scheme 1 is a simplified but typical representation of copper-catalysed ATRP. The copper(I) complex ($Cu^{I}L$) abstracts a halogen atom (X) from an alkyl-halide (RX) releasing a radical (R·) and the corresponding, halido-copper(II) complex ($Cu^{II}LX$). This step is coined 'activation' (with rate constant k_{act}). Subsequently the radical triggers propagation reactions (rate k_p) with olefin monomers to give the desired polymeric product. This process is tempered by the reverse 'deactivation' reaction (k_{deact} » k_{act}) which regenerates the dormant alkyl halide and the copper(I) complex. The equilibrium of this activation/deactivation reaction strongly favours the reactants and the concentration of R· is kept deliberately low to avoid unwanted side reactions such as bimolecular termination (2 R· → R-R).

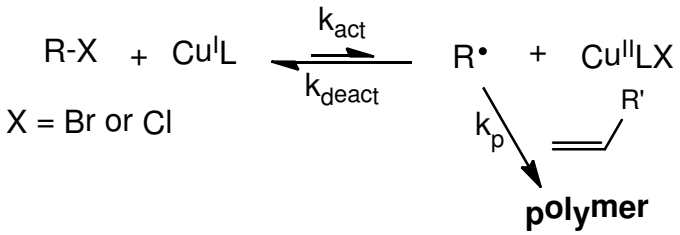

Scheme 1: Elementary reactions in copper catalysed ATRP (charges omitted for simplicity).

Two of the most active copper(I) complexes for ATRP ($Cu^{I}L$) bear the chelating ligands tris[2-(dimethylamino)ethyl]amine (Me_6tren)[5-7] and N,N,N′,N′,N″-pentamethyldiethylenetriamine (PMDETA).[8-10] Their five-coordinate 'deactivating' halido-copper(II) complexes ($Cu^{II}LX$ in Scheme 1) have been crystallographically characterized (Figure 1) and they exhibit trigonal bipyramidal (Me_6tren)[11] or square based pyramidal (PMDETA) coordination geometries.[12] The trigonal bipyramidal $[Cu^{II}(Me_6tren)X]^+$ (X = Cl, Br) complexes bear a single tightly bound halido ligand in an axial position. By contrast the square pyramidal $[Cu(PMDETA)X(Y)]^+$ complexes (X = F, Cl, Br; Y = solvent) comprise a strongly bound equatorial halido ligand and a weakly bound axial ligand due to the (pseudo) Jahn Teller effect.[13] The weak axial Cu--Y bond is represented by a broken line in Figure 1.

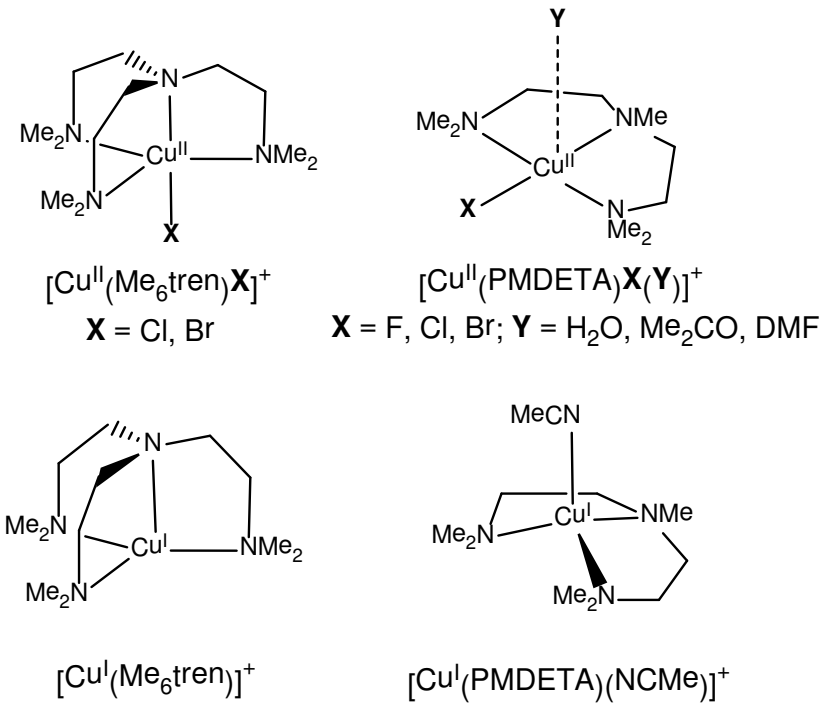

Figure 1: Structurally characterized copper(II) and copper(I) complexes relevant to this work.

There are only two structurally characterized Cu(I) complexes of Me_6tren extant, [Cu(Me_6tren)](ClO_4)[14] and [Cu(Me_6tren)](BPh_4),[15] which both are both 4-coordinate (Figure 1). In the case of the tridentate PMDETA all crystallographically characterized Cu(I) complexes are found in a distorted tetrahedral geometry such as [Cu(PMDETA)(MeCN)](ClO_4)[16] (Figure 1) as well as a series of η^2-coordinated olefin complexes [Cu(PMDETA)(Y)](BPh_4) (Y = styrene, octene, methyl acrylate).[17] It should be remembered that these are crystal structures and do not necessarily correspond to the solution structure when solvents or other ligands may enter the coordination sphere.

Relating these complexes to Scheme 1, it is noteworthy that the stringent condition of an atom transfer mechanism is that the coordination number of the active Cu(I) catalyst must increase by one in forming the halido-coordinated copper(II) complex. From Figure 1 it is evident that the well characterised Cu(II) complexes of Me_6tren and PMDETA are strictly 5-coordinate (Figure 1); the steric demands of the methylated amines blocking the entry of any additional ligands. Therefore the *active* copper(I) complex must be four-coordinate complex *bearing no halide ligands* in order for the reaction to be truly catalytic (see Scheme 2).

It has recently been reported that the activation reaction in Scheme 1 can be electrochemically triggered and the ratio of Cu(II)/Cu(I) complex controlled potentiostatically beginning with a bulk solution of dormant $[Cu^{II}LX]^+$.[18] Our own work has demonstrated that activation may be driven electro-catalytically.[19] Both of these studies employed $[Cu^{II}(Me_6tren)Br]^+$ as the starting complex.

Given that the copper(I) complexes of Me_6tren in the presence and absence of bromide ions are oxidised at distinctly different potentials,[19] it is clear that bromide is a competitive ligand for Cu(I) (as well as Cu(II)). This immediately creates a problem in that these $Cu^{I}LX$ (X = halide) complexes will be unreactive towards an initiator RX. Electrochemical or chemical reduction of the copper(II) complex in Scheme 1 ($[Cu^{II}LX]^{+}$) will yield $[Cu^{I}LX]$. So ligand dissociation (from $[Cu^{I}LX]$ to $[Cu^{I}L]^{+}$) must precede activation.[20] This reaction is critical in accounting for removal of the halido ligand in each cycle of the reaction. Halido ligand dissociation from copper(I) complexes has been overlooked as a potential rate determining step in the kinetics of ATRP (Scheme 1).

The copper-PMDETA complex also exhibits a number of interesting properties in terms of its atom transfer activation chemistry. In the current work we investigate how the solvent exhibits a strong influence on the rate of activation for this complex. For the first time, we separate the copper(I) ligand dissociation step (generating $[Cu^{I}L]^{+}$) from the true atom transfer activation step (Scheme 2) and in doing so we are able to understand the solvent dependence of k_{act} in the Cu/PMDETA system.

2. Experimental

2.1 Physical Methods

2.1.1. Spectrophotometric Titrations

UV-vis spectra were acquired with a Perkin Elmer Lambda 35 spectrophotometer. Spectrophotometric titrations of bromide into DMSO and MeCN solutions of $[Cu^{II}(PMDETA)(ClO_4)_2]$ were conducted using matching quartz cuvettes. The experimental cuvette contained 3 mL of 1 mM $[Cu^{II}(PMDETA)(ClO_4)_2]$ in DMSO or MeCN (with 0.1 M Et_4NClO_4 as inert electrolyte) and the reference cuvette contained 3 mL of the relevant DMSO or MeCN solution. Into both the experimental and reference cuvettes was titrated 10% equivalents of bromide via a concentrated Et_4NBr stock solution in DMSO or MeCN (34 mM Et_4NBr, 8.82 µL aliquots) and the absorbance spectra were measured from 450 nm – 1100 nm after each addition. Data were modelled using global analysis with the program ReactLab Equilibria.[21]

2.1.2 Electrochemistry

Cyclic voltammetry was performed on a BAS100B/W potentiostat employing a glassy carbon working electrode, platinum auxiliary electrode and a non-aqueous Ag/Ag^+ reference electrode in the solvent of choice (DMSO or MeCN). Ferrocene was used as an internal standard and all potentials are cited versus $Fc^{+/0}$. The supporting electrolyte was 0.1 M Et_4NClO_4 and all solutions were purged with nitrogen before measurement. 10 mL solutions of 1 mM $[Cu^{II}(PMDETA)Br_2]$ in DMSO and MeCN were employed in the electrochemical cell for experiments investigating the catalytic voltammetry in the presence of increasing concentrations of ethyl-α-bromoisobutyrate (EBriB). For experiments investigating the effect of free bromide on catalytic voltammetry in DMSO, 5 mL of 1 mM $[Cu^{II}(PMDETA)Br_2]$ in DMSO was utilized. Initially the cell was charged with 5 mM EBriB to stimulate catalytic voltammetry and then sequential 28.6 µL aliquots of 350 mM Et_4NBr in DMSO were titrated to increase the concentration of bromide in the cell by 2 mM increments up to a total concentration of 17 mM Br^-. Simulation of cyclic voltammetry was carried out with the program DigSim version 3.0.[22]

2.1.3. Electron Paramagnetic Resonance Spectroscopy

EPR spectra were measured with a Bruker ER200 instrument at X-band frequency (~9.4 GHz) as frozen 1 mM MeCN & DMSO solutions at 150 K. Spin Hamiltonian parameters were determined by spectral simulation with the program EPR50F.[23]

2.2 Synthesis

Safety Note- Perchlorate salts are potentially explosive. Although no problems were encountered with the compounds in this work they should never be heated in the solid state or scraped from sintered glass frits.

All solvents and reagents were obtained commercially (including PMDETA ligand, Aldrich 99%) and used without further purification.

$[Cu^{II}(PMDETA)(ClO_4)_2].H_2O$

A solution of PMDETA (0.0887 g, 0.49 mmol) in EtOH (10 mL) was added drop-wise to a solution of $Cu^{II}(ClO_4)_2.6H_2O$ (0.182 g, 0.49 mmol) in hot ethanol (10 mL). A deep blue solution ensued. The solution was stirred at ~60°C for 10 minutes before being allowed to cool to room temperature. Diethyl ether (20 mL) was added slowly and the suspension placed in the fridge overnight. The resulting blue solid was filtered off and dried (0.178 g. 80 % yield). Anal. Calcd. For $C_9H_{23}O_9N_3CuCl_2$ (453.77 $gmol^{-1}$): C, 23.8; H, 5.55; O, 31.7; N, 9.26. Found: C, 23.6; H, 5.93; O, 32.0; N, 9.19. Solvent complexes $[Cu^{II}(PMDETA)(sol)_2](ClO_4)_2$ (sol = DMSO or MeCN) were prepared *in situ* by dissolving $[Cu^{II}(PMDETA)(ClO_4)_2].H_2O$ in the relevant solvent.

$[Cu^{II}(PMDETA)Br_2]$

This complex was prepared by addition of PMDETA (0.177 g, 1 mmol) to $CuBr_2$ (0.223 g, 1 mmol) suspended in CH_2Cl_2 (20 mL). The solid was precipitated by slow addition of diethyl ether. The product was filtered off and washed with cold diethyl ether to remove any residual ligand (0.301 g, 76 % yield). X-ray quality crystals of $[Cu^{II}(PMDETA)Br_2]$ were obtained by diffusion of diethyl ether into an ethanol solution of the complex at ~2˚C. The crystal structure of this complex has been published previously[12] and the present complex was identical from X-ray analysis (data not shown). Anal. Calcd for $C_9H_{23}CuN_3Br_2$: C, 27.25; H, 5.80; N, 10.60. Found: C, 26.95; H, 5.89; N, 10.51.

3. Results and Discussion

3.1 Solution structure of [Cu(PMDETA)Br_2]

The crystal structure of the di-bromido complex [Cu^{II}(PMDETA)Br_2][12] reveals that the halide ligands complete a five-coordinate coordination sphere with a square-based pyramidal geometry. The bromide that occupies the equatorial position exhibits a shorter bond (Cu-Br 2.4462(9) Å) than the axially coordinated bromide (Cu-Br 2.6442(9) Å),[12] as expected from analogous complexes (see Figure 1). Elongated axial coordinate bonds are nearly always found in Cu^{II} complexes bearing square-pyramidal or six-coordinate octahedral coordination geometries due to the Jahn Teller effect[13, 24] where the degeneracy of the formally antibonding $d_{x^2-y^2}$ and d_{z^2} orbitals is removed by this distortion. In line with other mixed ligand complexes of formula [Cu^{II}(PMDETA)X(Y)]$^+$ (X = halide, Y = solvent, Figure 1) the weakly bound axial solvent ligand is easily displaced (broken lines, Figure 1). This weak axial ligand has little influence on the reactivity of the Cu(II) complex and in fact it dissociates completely on reduction to four coordinate Cu(I).

3.1.1 Electronic Spectroscopy

Spectrophotometric titrations of bromide into solutions of [Cu(PMDETA)]$(ClO_4)_2$ were performed to quantify bromide complexation and to determine the magnitude of the resulting association constants ($K_{Cu(II)Br}$) in competition with the solvent. Starting with [Cu^{II}(PMDETA)]$(ClO_4)_2$, where the ClO_4^- anions are effectively non-coordinating, the electronic spectra in MeCN and DMSO were consistent with [Cu^{II}(PMDETA)$(sol)_2$]$^{2+}$ (sol = MeCN or DMSO). The complex [Cu^{II}(PMDETA)$(MeCN)_2$]$^{2+}$ has been structurally characterized, bearing one strong (equatorial) and one weak (axial) MeCN ligand.[25] The MeCN complex exhibits a higher energy *d-d* transition from the stronger ligand field N-donor compared with the O-donor DMSO (Figure 2 – Table 1).

Spectrophotometric titration of bromide (as Et_4NBr) into each solution resulted in bathochromic shifts in the absorbance maxima consistent with replacement of the O- or N-donor solvent ligands with the weaker field bromido ligand (Table 1). Importantly, these titrations were both complete after the addition of *one equivalent* of bromide. Furthermore, the final spectra of the bromide complexes in MeCN and DMSO were clearly different. From the apparent 1:1 Cu(II):Br^- stoichiometry, only one of the solvent ligands is substituted by bromide. The presence of a residual solvent ligand is confirmed by the distinctly different electronic maxima of [Cu^{II}(PMDETA)Br(MeCN)]$^+$ and [Cu^{II}(PMDETA)Br(DMSO)]$^+$ (Figure 2 – Table 1) that arise from the disparate ligand field strengths of MeCN and DMSO.

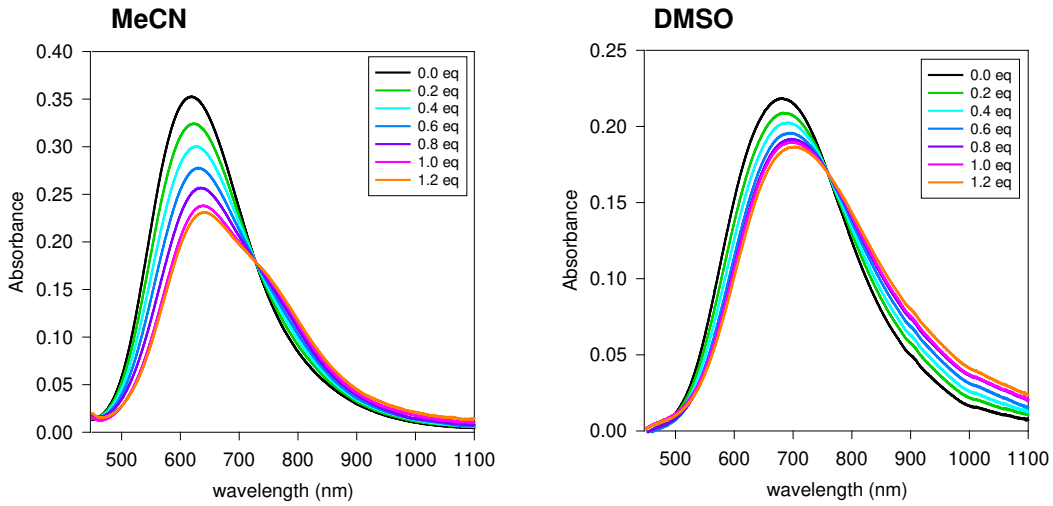

Figure 2: Spectrophotometric titrations of bromide (as Et_4NBr) into solutions of 1 mM $[Cu^{II}(PMDETA)(sol)_2](ClO_4)_2]$ (sol = DMSO and MeCN). The figure legend indicates stoichiometric amounts of bromide added. Supporting electrolyte 0.1 M Et_4NClO_4.

Table 1: Spectrophotometric titration data for bromide association in the Cu/PMDETA system.

Sol	$[Cu^{II}(PMDETA)(sol)_2]^{2+}$	$[Cu^{II}(PMDETA)Br(sol)]^{+}$	$logK_{Cu(II)Br}$ [a]	$logK_{Cu(I)Br}$ [b]
MeCN	λ_{max} 620 nm	λ_{max} 650 nm	4.4 ± 0.1	1.6 ± 0.1
DMSO	λ_{max} 680 nm	λ_{max} 700 nm	3.56 ± 0.04	3.24 ± 0.04

[a] see equation (1); [b] determined using equation (2) and cyclic voltammetry data (section 3.2.1).

The crystal structures of a number of copper(II)-PMDETA complexes with halido and solvent co-ligands are known (see Figure 1).[26-28] In all cases the halido ligand is found in the equatorial plane (strongly bound) along with the tridentate coordinated PMDETA while the weakly bound axial ligand is either a solvent molecule or the remaining counter ion (see Figure 1).[12] This is also consistent with solution-based EXAFS analyses.[29] By analogy we conclude that the bromido ligand (in solution) binds exclusively in the equatorial coordination site in both MeCN and DMSO while the solvent occupies the axial coordination site.

Modelling the spectrophotometric titration data with ReactLab EQUILIBRIA[21] (global analysis of the entire spectrum) yielded the formation constants for the copper(II)-bromido complexes relative to their copper(II)-solvent complexes (Table 1). Note that the solvent concentration is omitted from the equilibrium expression (eq. 1).

$$K_{Cu(II)Br} = \frac{[[Cu^{II}LBr(sol)]^{+}]}{[[Cu^{II}L(sol)_2]^{2+}][Br^{-}]} \qquad \text{(sol=MeCN, DMSO)} \qquad (1)$$

The formation constants in Table 1 are comparable to other studies with the Cu^{II}/PMDETA system under somewhat different conditions.[30] Furthermore, addition of excess bromide (up to 25 equivalents) to $[Cu^{II}(PMDETA)Br(sol)]^+$ had no effect on the electronic spectrum, so partial PMDETA dissociation from Cu(II) can be discounted and only two Cu(II) complexes, $[Cu^{II}(PMDETA)(sol)_2]^{2+}$ and $[Cu^{II}(PMDETA)Br(sol)]^+$, are relevant.

3.1.2 EPR Spectroscopy

Further analyses of the solution-based structures of the $[Cu^{II}(PMDETA)Br(sol)]^+$ complexes were undertaken using EPR spectroscopy. The EPR spectra of frozen (150 K) 1 mM solutions of $[Cu^{II}(PMDETA)Br(sol)]Br$ (sol = DMSO and MeCN) in the presence of 0.1 M Et_4NClO_4 were measured to probe their structure in solution (Figure 3). The spectra are comparable to previously published results for analogous Cu^{II}-PMDETA complexes where a square-pyramidal geometry was assigned.[31, 32]

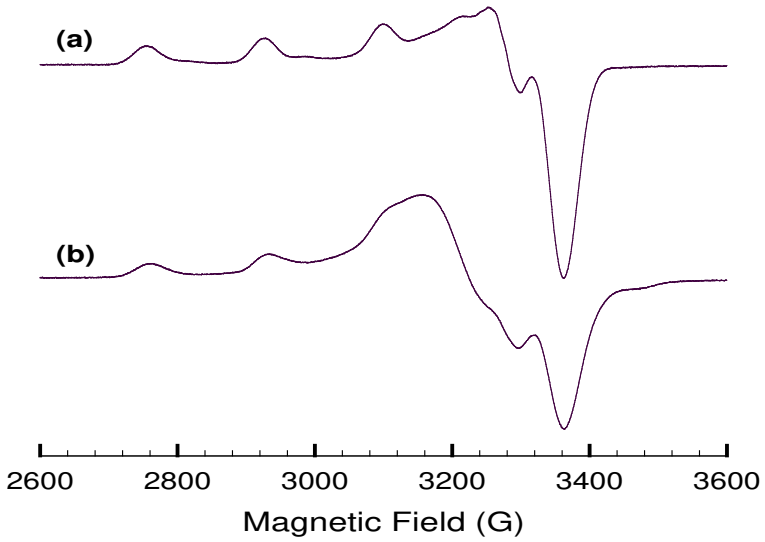

Figure 3: X-band (9.432 GHz) 150 K EPR spectra of $[Cu^{II}(PMDETA)Br(sol)]^+$ complexes in (a) DMSO & (b) MeCN. Spin Hamiltonian paramaters: $[Cu^{II}(PMDETA)Br(DMSO)]^+$ g_x 2.030 (A_x 25 G), g_y = 2.061 (A_y 25 G), g_z 2.236 (A_z 173 G); $[Cu^{II}(PMDETA)Br(MeCN)]^+$ g_x 2.070 (A_x 30 G), g_y = 2.070 (A_y 30 G), g_z 2.230 (A_z 175 G).

The EPR spectra of $[Cu^{II}(PMDETA)Br(sol)]^+$ in DMSO and MeCN are evidently not the same (Figure 3). The spin Hamiltonian parameters (obtained by simulation) differ slightly although in both cases they are consistent with a five-coordinate square pyramidal geometry (g_z » g_x, g_y; A_z » A_x, A_y) with the unpaired electron residing in an orbital with predominantly d_{x2-y2} character. The differences in the measured EPR are attributable to the axially coordinated solvent molecules (DMSO or MeCN), which is consistent with the electronic spectroscopy results (section 3.1.1, Figure 2).

3.2 Cyclic Voltammetry

3.2.1 Bromide/solvent competition

In parallel with the electronic spectroscopy experiments, the $[Cu^{II}(PMDETA)(sol)_2]^{2+}$ and $[Cu^{II}(PMDETA)Br(sol)]^{+}$ complexes could be observed separately with cyclic voltammetry as they are reduced at different potentials. Starting again with the $[Cu^{II}(PMDETA)(sol)_2]^{2+}$ complex a quasi-reversible $Cu^{II/I}$ couple was observed in each solvent (Figure 4(a) and 4(b) 0 eq. Br^-). With increasing additions of bromide this wave was gradually replaced by a lower potential wave corresponding to the Cu(II/I) couple of the bromido complex. After the addition of one equivalent of bromide there was no further change to the voltammogram in either DMSO or MeCN which is consistent with the spectrophotometric titration data which showed a 1:1 bromide:copper stoichiometry.

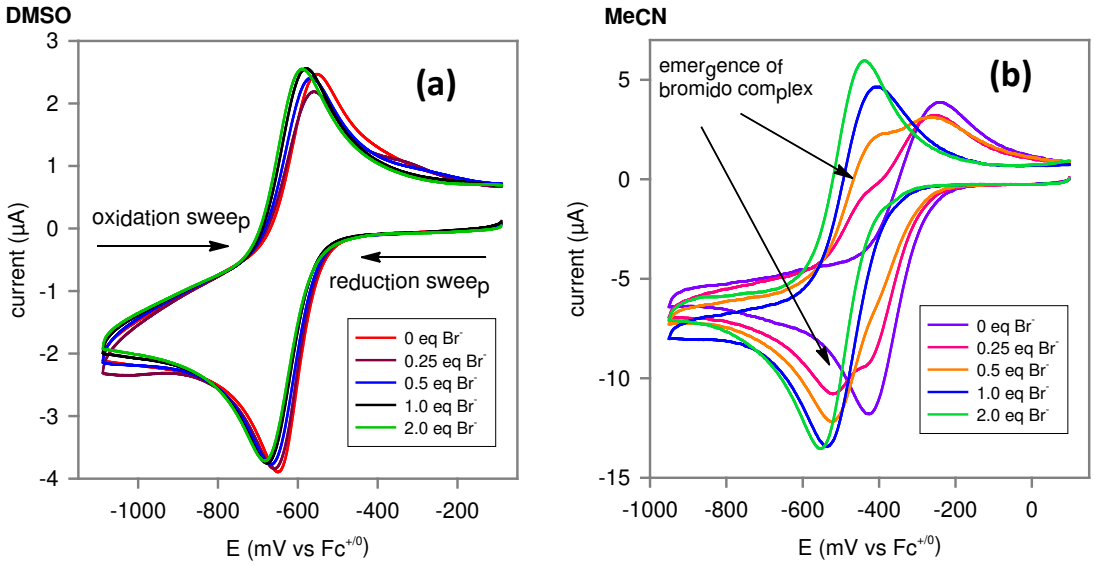

Figure 4. Cyclic voltammograms of (a) $[Cu(PMDETA)(DMSO)_2]^{2+}$ and (b) $[Cu(PMDETA)(MeCN)_2]^{2+}$ with bromide (0.1 M Et_4NClO_4).

The most obvious difference between the experiments carried out in DMSO and MeCN was the redox potential shift upon bromide complexation. In MeCN (Figure 4(b)) a pronounced shift of -166 mV was seen upon bromide complexation to give two well separated couples while in DMSO (Figure 4(a)) the shift was very small (-19 mV) with the two waves almost completely overlapping.

There is another important point to note. The presence of separate anodic peaks (of equal magnitude to the corresponding cathodic peak) illustrates that both $[Cu^{I}(PMDETA)Br]$ and $[Cu^{I}(PMDETA)(sol)]^{+}$ (sol = MeCN or DMSO) are stable on the voltammetric timescale and ligand exchange is slow to the point that they may coexist.

3.2.2 Catalytic mechanism

All electrochemical studies utilised $[Cu^{II}(PMDETA)Br(sol)]^+$ (sol = MeCN or DMSO) as the dominant starting species in the electrochemical cell. An extra equivalent of free bromide is also present from the $[Cu^{II}(PMDETA)Br_2]$ starting material which dissociates to $[Cu^{II}(PMDETA)Br(sol)]^+$ and Br^- (see sections 3.1.1 and 3.1.2).

The kinetics of ligand exchange reactions in the Cu^I/PMDETA system are not easily studied directly because the Cu(I) complex is highly reactive; prone to disproportionation and air sensitive.[16, 33] We have recently reported[19] a robust technique for investigating the kinetics of reactions such as these under strict anaerobic conditions of ATRP employing stable Cu^{II} precursors. In this case we have used $[Cu^{II}(PMDETA)Br(sol)]^+$ (sol = MeCN, DMSO). Through cyclic voltammetry (CV), it is possible to generate the active copper(I) complex electrochemically and probe its response to an alkyl-halide initiator. Scheme 2 illustrates this reaction sequence.

The coordination number of all Cu(II) PMDETA complexes is undoubtedly five from existing crystallographic and spectroscopic (UV-Vis and EPR) evidence. The coordination number of the spectroscopically silent Cu(I) complexes is more difficult to characterize. On the basis of existing solid state structural evidence it seems likely that all Cu(I) complexes of PMDETA exhibit a distorted tetrahedral geometry. This can be easily reconciled here by assuming that the weakly bound axial solvent ligand bound to Cu(II) dissociates upon reduction to Cu(I).

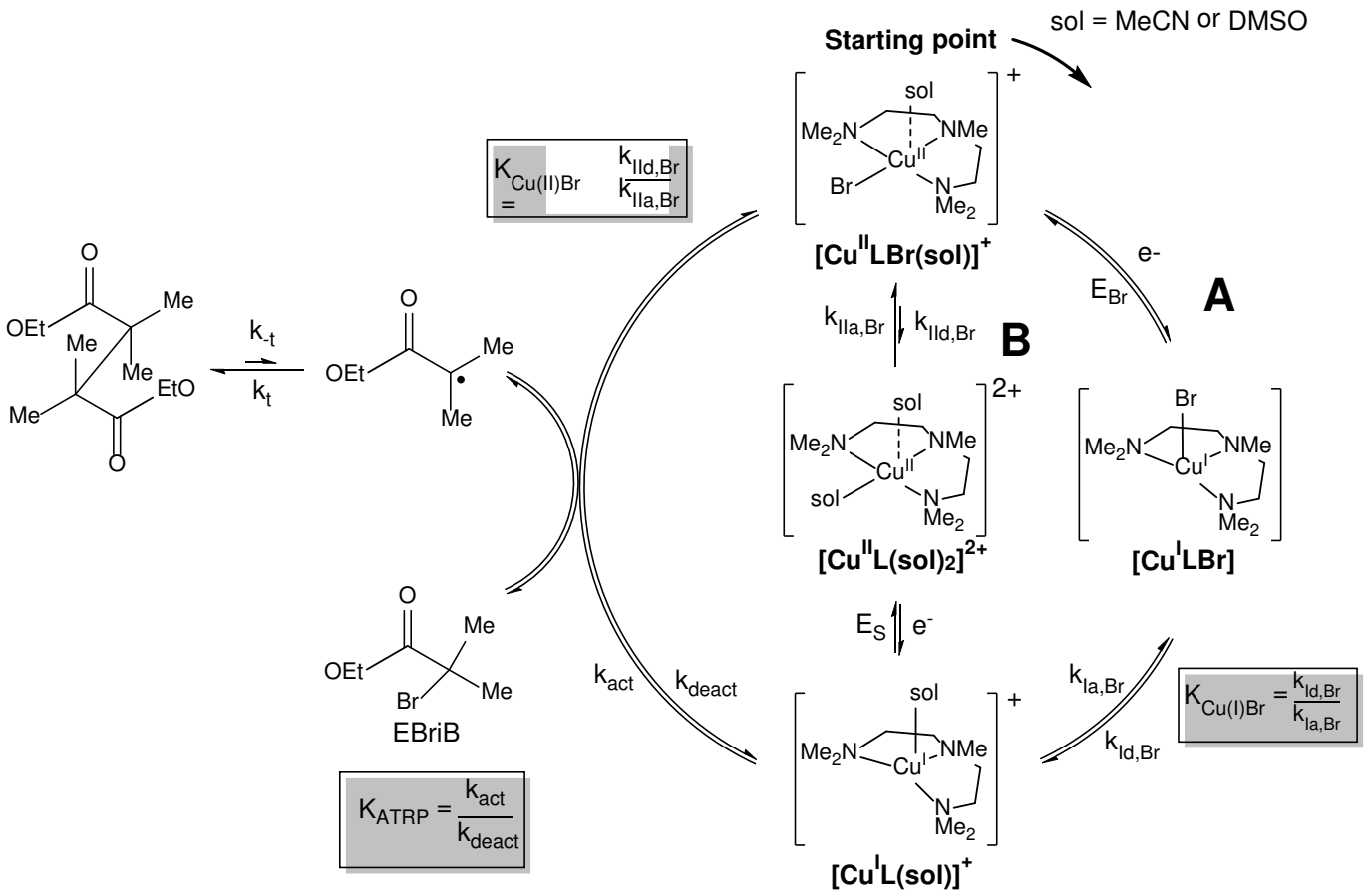

Scheme 2: Electrochemically driven Cu-catalysed atom transfer reactions of Cu(II/I) PMDETA (an EC_{cat} activation reaction).

3.2.3 Catalytic voltammetry of [Cu^{II}(PMDETA)Br(sol)]Br (sol = DMSO and MeCN)

The cyclic voltammetry of $[Cu^{II}(PMDETA)Br(DMSO)]^+$ in a DMSO solution of the initiator ethyl bromoisobutyrate (EBriB) is shown in Figure 5(a). These CVs exemplify the electro-catalytic activation reaction. During the initial cathodic sweep $[Cu^{II}(PMDETA)Br(DMSO)]^+$ and $[Cu^{II}(PMDETA)(DMSO)_2]^{2+}$ (in pre-equilibrium) are reduced to their corresponding Cu(I) complexes $[Cu^{I}(PMDETA)Br]$ (at E_{Br}) and $[Cu^{I}(PMDETA)(DMSO)]^+$ (at E_S). In the *absence* of an alkyl-halide initiator (red curve, 0 eq EBriB), the anodic sweep regenerates the starting species and a quasi-reversible voltammogram is observed as also illustrated in Figure 4(a). Although bromide dissociation from the Cu(II) complex is significant (~20%) the two redox couples E_{Br} and E_S essentially overlap (Table 2, Figure 4(a)) so separate responses from $[Cu^{II}(PMDETA)Br(DMSO)]^+$ and $[Cu^{II}(PMDETA)(DMSO)_2]^{2+}$ cannot be resolved.

In the presence of EBriB (RX in Scheme 1) the active four-coordinate catalyst $[Cu^{I}(PMDETA)(sol)]^+$, in equilibrium with $[Cu^{I}(PMDETA)Br]$ (Scheme 2), is consumed by EBriB in the coupled activation

reaction (k_{act}) to regenerate the starting species $[Cu^{II}(PMDETA)Br(sol)]^+$ releasing an alkyl radical. Regeneration of $[Cu^{II}(PMDETA)Br(sol)]^+$ results in amplification of the cathodic wave at the potential E_{Br} (Figure 5(a)) which is characteristic of an EC_{cat} voltammogram. The anodic (reoxidation) current is diminished due to the removal of $[Cu^{I}(PMDETA)(DMSO)]^+$, which is in equilibrium with the bromido complex $[Cu^{I}(PMDETA)Br]$.

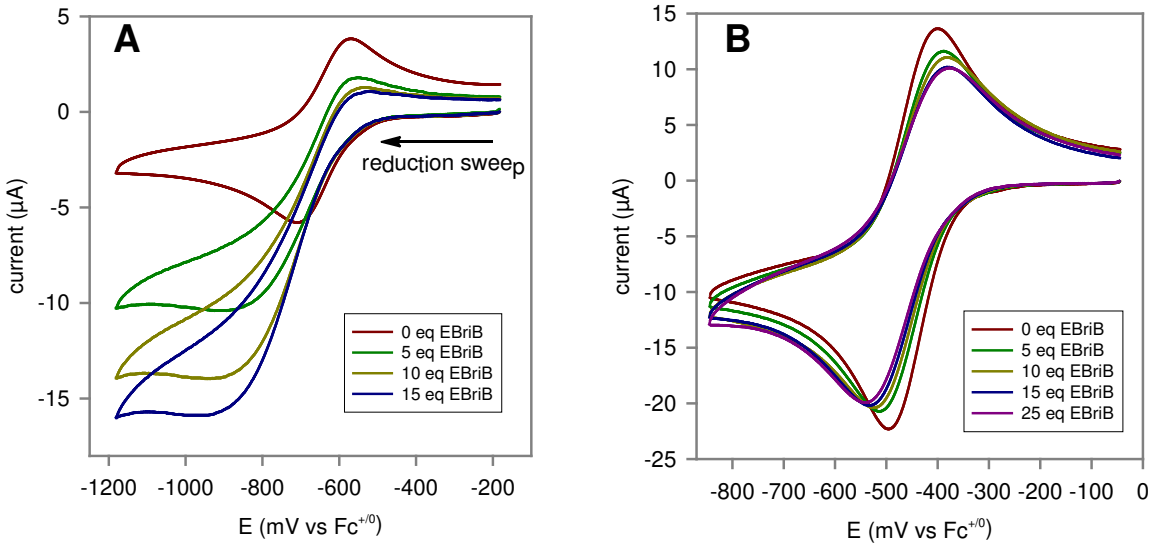

Figure 5: Solvent dependent cyclic voltammetry of (**A**) 1 mM $[Cu^{II}(PMDETA)Br(DMSO)]^+$ (in DMSO, sweep rate 50 mV s^{-1}) and (**B**) 1 mM $[Cu^{II}(PMDETA)Br(MeCN)]^+$ (in MeCN, sweep rate 100 mV s^{-1}) in the presence of increasing equivalent amounts of EBriB.

Table 2: Rate constants and redox potentials for the Cu/PMDETA/EBriB system (see Scheme 2).

	MeCN	**DMSO**
k_{deact} **(M^{-1} s^{-1})**	5.00×10^7	5.00×10^7
k_{act} **(M^{-1} s^{-1})**	7.33×10^3	7.33×10^3
$k_{IId,Br}$ **(s^{-1})**	0.37	0.28
$k_{IIa,Br}$ **(M^{-1} s^{-1})**	7.43×10^3	1.00×10^3
$k_{Id,Br}$ **(s^{-1})**	0.08	12.0
$k_{Ia,Br}$ **(M^{-1} s^{-1})**	3.18	2.02×10^4
E_S **(mV vs. $Fc^{+/0}$)**	-334	-611
E_{Br} **(mV vs. $Fc^{+/0}$)**	-510	-630

The same experiments were performed with $[Cu^{II}(PMDETA)Br(MeCN)]^+$ in MeCN. In the absence of EBriB a quasi-reversible CV was observed (Figure 5(b)). The $Cu^{II/I}$ redox couple in MeCN appears at a different potential to that found in DMSO (Table 2). This is due to a combination of differences in inner sphere (coordination of MeCN *vs* DMSO to Cu) and outer sphere solvation effects. Importantly, and in contrast to DMSO, bromide dissociation from $[Cu^{II}(PMDETA)Br(MeCN)]^+$ is negligible in MeCN (~4%, Table 1) and only a single wave is observed.

However, in MeCN, the voltammogram is virtually insensitive to the presence of EBriB (Figure 5(b)). This indicates that activation in MeCN is suppressed relative to DMSO. This parallels the solvent dependence reported for ATRP activation with Cu/PMDETA in DMSO *versus* MeCN where the overall activation reaction is much slower in DMSO than MeCN.[34, 35]

3.2.4 Electrochemical simulation

Recently we employed[19] electrochemical simulation (using the program DigiSim[22]) to probe atom transfer radical activation and obtain accurate kinetics parameters for the Cu/Me_6tren system. Briefly, the kinetic and thermodynamic parameters in the model (Scheme 2) are optimized until agreement between the experimental and calculated voltammograms is obtained. Many of these parameters are determined accurately and independently in the absence of coupled catalytic reactions *e.g.* redox potentials, diffusion coefficients and heterogeneous electron transfer rate coefficients. The key variables are the homogeneous rate constants e.g. k_{act}, k_{deact} and bromide dissociation/association rate constants (Scheme 2) which were optimised across a range of EBriB concentrations and sweep rates in order to generate accurate values for these parameters which are shown in Table 2.

There are two pathways that the reaction mechanism may take starting from the Cu(II) complex of PMDETA. The first involves reduction of 5-coordinate $[Cu^{II}(PMDETA)Br(sol)]^+$ (with concomitant dissociation of the weakly bound solvent) to afford 4-coordinate $[Cu^{I}(PMDETA)Br]$ followed by bromide substitution by solvent to generate the active catalyst $[Cu^{I}(PMDETA)(sol)]^+$ (pathway **A**). The alternative pathway begins with $[Cu^{II}(PMDETA)(sol)_2]^{2+}$ (in pre-equilibrium with $[Cu^{II}(PMDETA)Br(sol)]^+$) which leads directly to $[Cu^{I}(PMDETA)(sol)]^+$ via a single electron reduction (pathway **B**). The model separates the bromido ligand dissociation and activation steps which have never been examined independently and the possibility that formation of the active 4-coordinate $[Cu^{I}(PMDETA)(sol)]^+$ complex may be rate limiting in the overall activation reaction has never been considered.

As with any multivariable fitting process, there is a danger of false minima. In order to obtain meaningful fits we constrained as many parameters as possible. E_{Br} was determined in the absence

of any coupled chemical reaction in both solvents along with the heterogeneous rate constants k_0 and the diffusion coefficients (4.6×10^{-6} cm^2 s^{-1} in DMSO and 2.9×10^{-5} cm^2 s^{-1} in MeCN), by simulating the voltammetry of $[Cu^{II/I}(PMDETA)Br(sol)]^+$ in both solvents without EBriB.

The measured Cu(II)-Br association constants in Table 1 indicate that $[Cu^{II}(PMDETA)Br(sol)]^+$ is the major species at the beginning of the sweep (and in bulk solution). The somewhat smaller bromide association constant in DMSO (Table 1) means that $[Cu^{II}(PMDETA)Br(DMSO)]^+$ is ~20% dissociated (into $[Cu^{II}(PMDETA)(DMSO)_2]^+$ and Br^-) at 1 mM total concentration, while in MeCN there is less than 4% bromide dissociation from Cu(II). However, as the Cu(II) system is at equilibrium at the start, there is no way of determining the kinetics of bromide dissociation/association on copper(II) so the absolute values of bromide association and dissociation rates ($k_{aII,Br}$ and $k_{dII,Br}$) for the Cu(II) complexes are arbitrary although their ratio ($K_{Cu(II)Br}$) was determined accurately by the spectrophotometric and electrochemical experiments (see sections 3.1.1 and 3.2.1 and Table 1).

The shift in Cu(II/I) redox potential going from the solvent coordinated complex (E_S) to bromide coordinated complex (E_{Br}) is related to the relative bromide association constants in the copper(II) and copper(I) forms (eq. 2). The equilibrium constants $K_{Cu(II)Br}$ and $K_{Cu(I)Br}$ correspond to the bromide complexation processes for the copper(II)-solvent and copper(I)-solvent complexes respectively. These expressions are substituted into the Nernst equation for the concentrations of the oxidised and reduced species resulting in equation 2. Given that $K_{Cu(II)Br}$ was determined spectrophotometrically (Section 3.1.1 and Table 1), this leads to the Cu(I)-Br association constants directly (Table 1).

$$\log\left(\frac{K_{Cu(II)Br}}{K_{Cu(I)Br}}\right) = 16.9(E_S - E_{Br}) \quad at\ 298K \qquad (2)$$

It is important to highlight that these Cu(I)-Br association constants are equally valid for bulk solutions of $[Cu^{I}(PMDETA)Br]$ in DMSO or MeCN. Whilst these values indicate that bromide binds to copper(I) in these two solvents, they also illustrate that the solvent has a major influence on the degree of bromide dissociation from the Cu(I) complex. In particular, $[Cu^{I}(PMDETA)Br]$ is significantly more stable in DMSO than in MeCN *at equilibrium*. However, given that the system is dynamic and the Cu(I) complexes are generated electrochemically the kinetics of this dissociation reaction ($k_{dI,Br}$) also need to be considered.

The radical termination step ($k_t = 10^9$ M^{-1} s^{-1}) is known to be diffusion controlled and irreversible[36] so the reverse rate coefficient (k_{-t}) is negligible. Here it was set to a nominally low value (1.3×10^{-3} s^{-1}) in accordance with work previously published.[19] The activation rate (k_{act}), representing the single step

for halogen abstraction in Scheme 2, was able to be set to a common value of 6.0×10^3 M^{-1} s^{-1} in both solvent systems and also the deactivation rate constant k_{deact} was set as 5.0×10^7 M^{-1} s^{-1} for both DMSO and MeCN *i.e.* $K_{ATRP} = 1.5 \times 10^{-4}$ regardless of solvent. We note that any differences in the apparent overall activation/deactivation rates in the past have been absorbed into a single parameter (K_{ATRP} – which is different from K_{ATRP} in Scheme 2).

Our hypothesis herein is that K_{ATRP} (k_{act}/k_{deact} from Scheme 2) is solvent *independent*, and thus k_{act} too is solvent independent given that there is very little variation in k_{deact} for a given complex and initiator. In doing this we propose that solvent influences that rate of formation of the active cationic species $[Cu^{I}(PMDETA)(sol)]^+$ via the neutral precursor $[Cu^{I}(PMDETA)Br]$ or from reduction of the Cu(II) complex $[Cu^{II}(PMDETA)(sol)_2]^+$ (depending on pathway **A** or **B** in Scheme 2). By exerting control over the pathway, the solvent modulates the production of the common active species $[Cu^{I}(PMDETA)(sol)]^+$. Moreover, once separated from the bromide dissociation step, the atom transfer (activation) reaction between $[Cu^{I}(PMDETA)(sol)]^+$ and EBriB (k_{act}), where the solvent does not actually participate, should not be strongly solvent dependent as no solvent ligands are exchanged during this step.

The value of K_{ATRP} which we incorporate in our studies is comparable with published values in DMSO and is consistent with values determined by analogous electrochemical investigations of $[Cu^{I}(Me_6tren)Br]$ ($k_{act} \sim 10^2 - 10^3$ M^{-1} s^{-1})[19] and the established lower activity of the copper/PMDETA catalyst compared to the copper/Me_6tren system.[34]

The only remaining variables to address in the simulations were the Cu(I)-Br dissociation/association rate constants which are linked by the known equilibrium constants $K_{Cu(I)Br}$ ($=k_{Ia,Br}/k_{Id,Br}$) in MeCN and DMSO. So $k_{Id,Br}$ or $k_{Ia,Br}$ were the only parameters which were allowed to vary. During the iterative fitting process for the MeCN system, $k_{aI,Br}$ began to decrease (relative to its value in DMSO) until it reached a minimum at a value of 3.2 M^{-1} s^{-1} (Table 2). The resulting excellent agreement between the simulated and experimental voltammograms is apparent in Figure 6. The fit was consistent across a range of sweep rates (50 - 300 mV s^{-1}) and concentrations of EBriB (0 – 25 mM). The values determined for $k_{Ia,Br}$ (3.2 M^{-1} s^{-1}) and thus $k_{Id,Br}$ (0.08 s^{-1}) indicate a relatively slow bromide association/dissociation equilibrium for the Cu^{I} complex in MeCN.

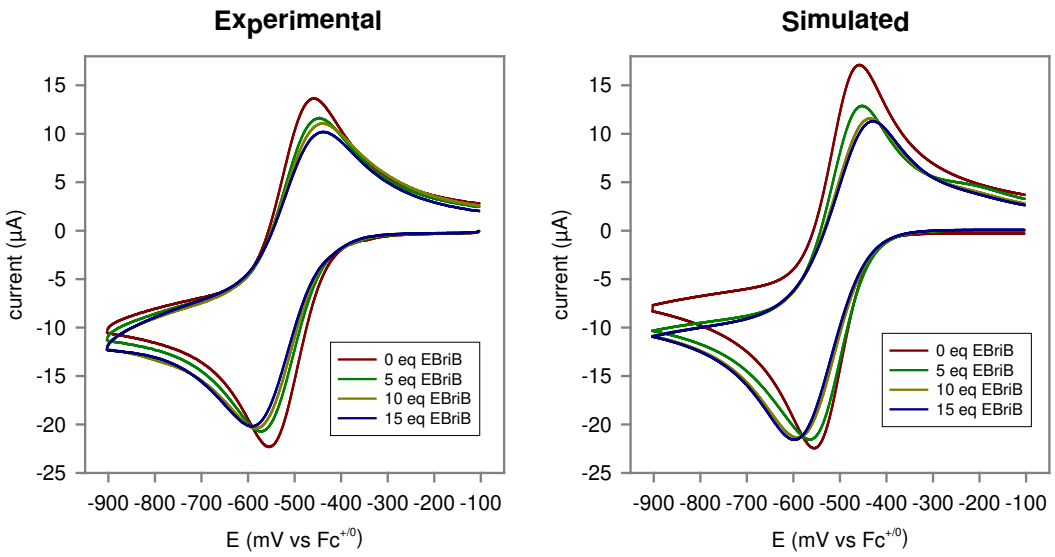

Figure 6: Comparison of simulated and experimental voltammetry of $[Cu^{II}(PMDETA)Br]^+$ in MeCN at a sweep rate of 100 mV s^{-1} with increasing alkyl EBriB.

By contrast, simulation of the DMSO system (Figure 7) furnished increasingly larger values of $k_{Ia,Br}$ during refinement until a final value of 2.2×10^4 M^{-1} s^{-1} was determined (and $k_{Id,Br}$ = 12 s^{-1} from the known value of $K_{Cu(I)Br}$). The resulting match between the calculated and experimental CVs was again excellent (Figure 7) and was consistent across a range of sweep rates (50 – 300 mVs^{-1}) and concentrations of EBriB (0 – 15 mM).

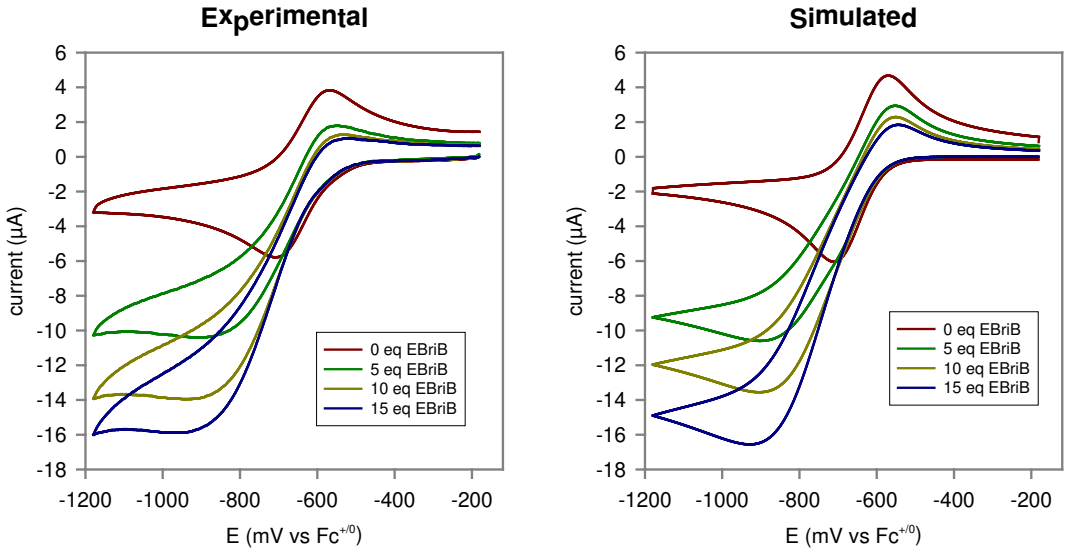

Figure 7: Comparison of simulated and experimental voltammetry of $[Cu^{II}(PMDETA)Br]^+$ in DMSO at a sweep rate of 100 mV s^{-1} with increasing concentration of EBriB.

It is essential that no reasonable fit to the experimental CVs could be achieved when the kinetics of bromide dissociation from copper(I) were constrained to be *similar* (i.e. $k_{Id,Br}$ (DMSO) ~ $k_{Id,Br}$ (MeCN)) even if k_{act} was allowed to vary. The three to four orders of magnitude difference in $k_{Id,Br}$ (going from MeCN to DMSO) and $k_{Ia,Br}$ is critical to understanding the differences in catalytic activation, and this could be modelled with a solvent independent value of k_{act}. In other words the activation step is not rate limiting despite the large differences in the overall reaction rate.

Before progressing further it is important to mention that the values for $k_{Ia,Br}/k_{Id,Br}$ in Table 2 are not necessarily absolute, but their order of magnitude is. These values are determined by a comparative fitting process where the variance between the simulated CVs and the experimental CVs is minimised. However the simulated CVs are not exact replicates of the experimental CVs and so there concurrently exists a degree of plausible variation in the kinetic values determined from these simulations which would still yield 'appropriate' fits. In reality then, changing the value of $k_{Id,Br}$ in MeCN from 0.08 s^{-1} to 0.06 s^{-1} has minimal effect on the fit. However adequate fits cannot be obtained when this value is changed to a number outside the order of magnitude 10^{-2} s^{-1}. So the three orders of magnitude difference between $k_{Id,Br}$ in DMSO versus MeCN is indisputably the origin of the clearly different rates of activation in these two solvents.

3.2.5 Speciation at the electrode surface:

This electrochemical study provides a novel insight into the kinetics of Cu-catalysed atom transfer radical reactions that is not possible through conventional chemical reactions of Cu(I) precursors where the Cu(I) complexes are already at equilibrium before the reaction begins. Recently, the potential for electrochemical mediation of ATRP reactions has been reported.[18, 37] Single electron transfer at the electrode to the copper(II) complex initiates the ATRP activation reaction, and after activation/polymerization has taken place, deactivation through reaction with the original copper(II)-bromido complex halts the reaction. It is thus of paramount importance to understand how the active catalyst $[Cu^{I}(PMDETA)(sol)]^{+}$ (sol = MeCN or DMSO) is formed subsequent to electron transfer and in particular what the kinetics are for this process.

One of the major advantages in having successfully simulated the catalytic electrochemical behaviour of the Cu/PMDETA system is the ability to produce a concentration profile of all species in Scheme 2 at the electrode surface at each potential along the voltammogram. However, this profile is more complex than a standard (bulk) solution concentration profile because it is distance dependent (from the electrode) and potential (time) dependent during the course of the CV. It was of particular interest to calculate the concentration profiles of the active catalyst $[Cu^{I}(PMDETA)(sol)]^{+}$ in both DMSO and MeCN.

At the commencement of the cathodic sweep, $[Cu^{II}(PMDETA)Br(sol)]^+$ prevails at the electrode surface when $E > E_{Br}$ in both DMSO and MeCN (Figure 8A and 8B). As the scan progresses (to the left of each figure), E_{Br} is reached and $[Cu^{I}(PMDETA)Br]$ is formed. In MeCN (Figure 8B), slow kinetics for the dissociation of bromide from $[Cu^{I}(PMDETA)Br]$ ($k_{Id,Br}$, $t_{1/2}$ ~8 s) limits the formation of $[Cu^{I}(PMDETA)(MeCN)]^+$ (red curve). $[Cu^{I}(PMDETA)(MeCN)]^+$ does not accumulate significantly in the concentration profile; its concentration peaks at ~0.02 mM then drops away as it is consumed by EBriB. As the concentration of $[Cu^{I}(PMDETA)(MeCN)]^+$ is low, minimal activation to give the radical-coupled dimer product (R-R, green curve) is found.

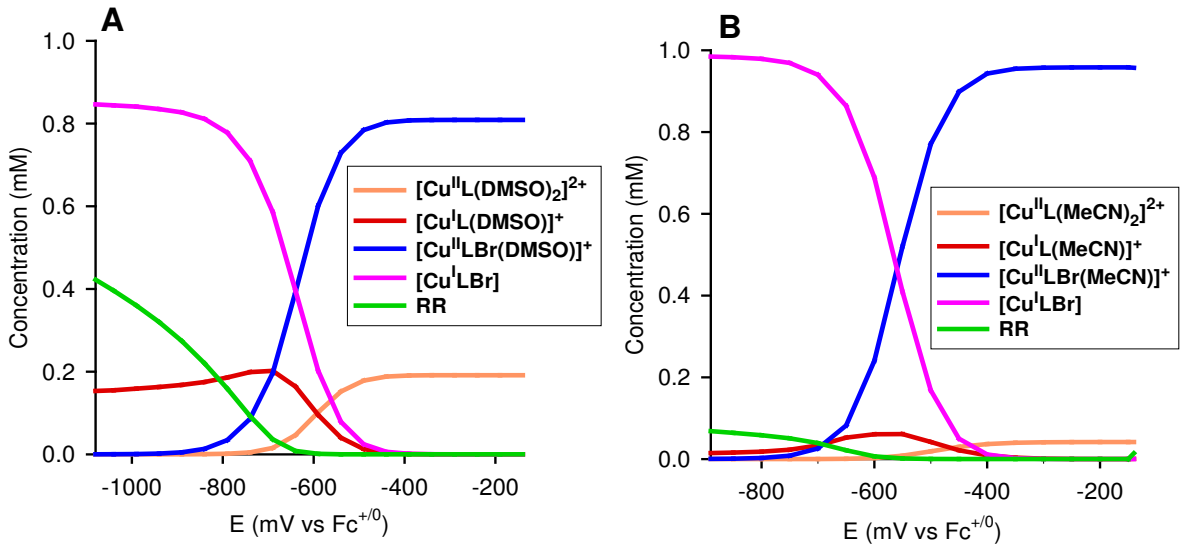

Figure 8: Speciation concentration profiles at the electrode surface (distance = 1 nm) during the cathodic sweep of electrochemically triggered atom transfer activation. (A) in DMSO and (B) in MeCN. Sweep rate is 50 mVs^{-1}, L = PMDETA; bulk concentrations: $[Cu(PMDETA)Br]^+$ = 1 mM; EBriB = 10 mM. Plots generated with Digisim.

In DMSO the formation of $[Cu^{I}(PMDETA)(DMSO)]^+$ is much more significant (Figure 8A). It may form directly via pathway **B** from reduction of $[Cu^{II}(PMDETA)(DMSO)_2]^{2+}$ (~ 20% present at the start of the sweep) or by rapid substitution of bromide by DMSO on $[Cu^{I}(PMDETA)Br]$ (pathway **A**). The resulting concentration of $[Cu^{I}(PMDETA)(DMSO)]^+$ plateaus at ~0.2 mM and remains constant (steady state) for the remainder of the reduction sweep. The concentration of the radical termination product R-R (Figure 8A green curve) increases rapidly during this part of the sweep and is about 10 times greater than in MeCN.

The concentration profiles for the DMSO and MeCN systems are only shown as two dimensional (concentration/potential) graphs at a fixed distance (~1 nm) from the surface of the electrode. With

the exception of $[Cu^{II}(PMDETA)Br(sol)]^+$ and to a lesser extent $[Cu^{II}(PMDETA)(sol)_2]^{2+}$ each of these species is insignificant beyond the diffusion layer (~1 mm).

3.2.6 Bromide inhibition

On the basis of bromide dissociation from Cu(I) being rate limiting, it follows that bromide is actually an inhibitor of atom transfer activation. To further support this hypothesis, the electrocatalytic behaviour of $[Cu^{II}(PMDETA)Br(DMSO)]^+$ and EBriB in DMSO was monitored in the presence of increasing concentrations of free bromide. According to Scheme 2, bromide inhibits catalysis by favouring formation of the inactive complex $[Cu^{I}(PMDETA)Br]$. Therefore the catalytic current should be suppressed as the concentration of bromide increases. This is in fact observed (Figure 9) where the catalytic voltammetry of $[Cu^{II}(PMDETA)Br(DMSO)]^+$ (in DMSO) in the presence of EBriB plus excess bromide reverts to voltammetry similar to that seen in the absence of EBriB altogether *i.e.* activation is completely suppressed. Simulations were again employed to support this proposed effect on the copper(I) equilibrium (Figure 9(b)).

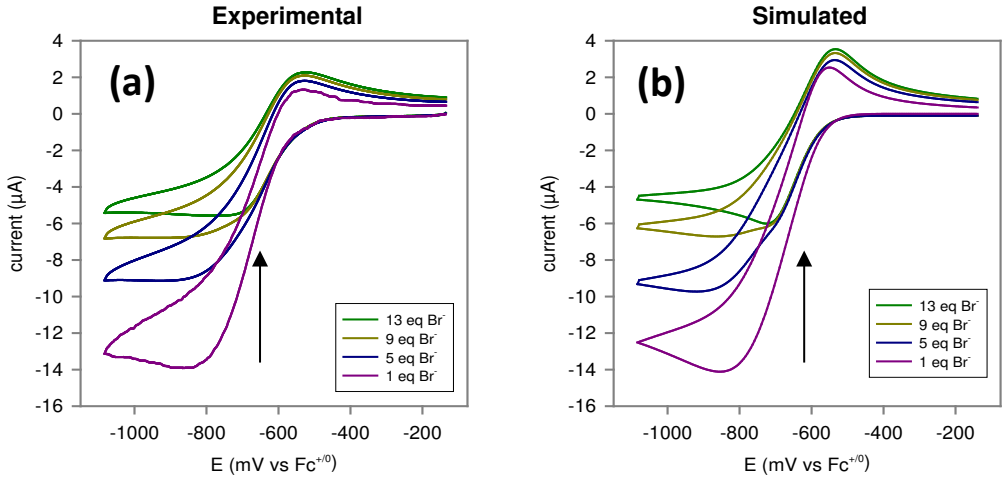

Figure 9: Comparison of (a) experimental and (b) simulated voltammetry at 50 mV s^{-1} for $[Cu^{II}(PMDETA)(Br)(DMSO)]^+$ (1 mM) with EBriB (5 mM) and increasing ratios of Br : Cu.

By utilising the same mechanism and parameters determined previously (Scheme 2 & Table 2), the experimental CVs were accurately reproduced as a function of increasing concentrations of bromide (Figure 9(b)). These experiments comprised a wide range of bromide concentrations (3- 19 mM) and sweep rates (20-300 mV s^{-1}). Given that the MeCN system was already virtually inactive under these conditions (Figure 5B), no meaningful bromide inhibition studies could be carried out.

3.3 Relevance to ATRP activation

Scheme 2 is the most comprehensive mechanism for electrochemically triggered activation within the copper/PMDETA system. We have observed that a single bromide binds to the copper(II)/PMDETA ion in both DMSO and MeCN even in the presence of a large excess of bromide. This means that the five coordinate complex $[Cu^{II}(PMDETA)Br(sol)]^+$, with solvent coordinated along with a single bromide, is the major species present at the start of the electrochemical reduction sweep. Furthermore, the Cu(II/I) redox potentials were clearly solvent dependent. This indicates that electrochemical reduction of this starting complex produces the corresponding copper(I)-bromido complex $[Cu^{I}(PMDETA)Br]$. Activation is clearly not possible directly from this compound because this would add a second bromido ligand and this species is not formed in solution as shown in Section 3.1.1. The key point is that bromide must be lost from the copper complex before activation can proceed.

In MeCN, $[Cu^{I}(PMDETA)(MeCN)]^+$ does not accumulate at the electrode (Figure 8(b)). Although the complex is still active, the rate at which it is formed at the electrode is too slow and it is consumed by EBriB more quickly than it can be regenerated. The spectrophotometric titrations indicated that bromide does not dissociate from $[Cu^{II}(PMDETA)Br(MeCN)]^+$ significantly at these concentrations so it emerges that electrochemical reduction leads directly to $[Cu^{I}(PMDETA)Br]$. Although bromide dissociation is spontaneous at 1 mM concentration ($K_{Cu(I)Br}$ ~ 40 M^{-1}) the kinetics of dissociation are surprisingly slow ($t_{1/2}$ > 8 s) and the dead end complex $[Cu^{I}(PMDETA)Br]^+$ accumulates at the electrode (Figure 8B). In terms of Scheme 2, pathway **A** is followed in MeCN and the reaction is under kinetic control by the rate of bromide ligand dissociation from Cu(I) to yield the active catalyst.

In DMSO the situation is quite different. At the outset, ~20% of bromide dissociation from the Cu(II) complex has already occurred ($K_{Cu(II)Br}$ ~ 3600 M^{-1}). As the potential is lowered $[Cu^{II}(PMDETA)(DMSO)_2]^+$ is converted directly into the active catalyst $[Cu^{I}(PMDETA)(DMSO)]^+$ without limitations from ligand substitution and this reacts with EBriB directly. Note the concentration of $[Cu^{I}(PMDETA)(DMSO)]^+$ at low potential is essentially the same as $[Cu^{II}(PMDETA)(DMSO)_2]^{2+}$ at high potential so one complex appears as the product of the other. Concomitantly the ~80% of $[Cu^{II}(PMDETA)Br(DMSO)]^+$ is reduced to $[Cu^{I}(PMDETA)Br]$ (again a dead end complex) but the much larger bromide association constant for this complex (Table 1, $K_{Cu(I)Br}$ ~ 1700 M^{-1}) limits further significant bromide dissociation to ~61% $[Cu^{I}(PMDETA)Br]$ (at equilibrium). So in this case both pathways **A** & **B** (Scheme 2) can contribute to production of the active catalyst although the tighter binding Cu(I)-Br in DMSO limits the amount of $[Cu^{I}(PMDETA)(DMSO)]^+$ formed through pathway **B**.

Thermodynamically controlled production of the active catalyst through pathway **B** is likely the major factor contributing to the high degree of activation in this solvent system.

Electrochemical and spectrophotometric titrations indicate that no other copper(II) species apart from $[Cu^{II}(PMDETA)Br(sol)]^+$ and $[Cu^{II}(PMDETA)(sol)_2]^{2+}$ are ever present in solution. Absolutely no evidence exists for partial ligand dissociation induced by bromide competition for the metal. Similarly in the voltammetry experiments, no more than two waves were ever seen which correspond to the Cu(II/I) couples of the bromide and solvent coordinated complexes *i.e.* there are only ever two Cu(I) PMDETA complexes generated, namely $[Cu^{I}(PMDETA)Br]$ and $[Cu^{I}(PMDETA(sol)]^+$.

Titrations of free bromide in the presence of EBriB quenched the catalytic activity of the system in DMSO and the kinetic parameters described in Scheme 2 modelled this process as well without the need for consideration of any new species. Bromide clearly inhibits formation of the active catalyst. This again is consistent with the speciation diagram where high concentrations of bromide eliminate all traces of $[Cu^{II}(PMDETA)(DMSO_2)]^{2+}$ and only the complexes $[Cu^{II}(PMDETA)Br(DMSO)]^+$ and $[Cu^{I}(PMDETA)Br]$ (a dead end) are formed during the sweep. All of this evidence reaffirms the notion that the four-coordinate complex $[Cu^{I}(PMDETA)(DMSO)]^+$ is the true active catalyst in this solvent.

One question remains unanswered. Why is the formation of $[Cu^{I}(PMDETA)(MeCN)]^+$ from $[Cu^{I}(PMDETA)Br]$ so much slower than the formation of $[Cu^{I}(PMDETA)(DMSO)]^+$ from $[Cu^{I}(PMDETA)Br]$? It is well known that MeCN has a high affinity for Cu^{I} (the stable complex $[Cu(MeCN)_4]^+$ being a good example) but in this case ionisation of the complex is very slow ($[Cu^{I}(PMDETA)Br] + MeCN \rightarrow [Cu^{I}(PMDETA)(MeCN)]^+ + Br^-$). Slow kinetics for ligand exchange reactions in acetonitrile for copper complexes of the related Me_6tren ligand has been reported previously[38] but little is known about the kinetics of these exchange reactions for the PMDETA complex. It may be that ion pairing in the lower polarity MeCN solvent slows dissociation of the complex relative to the more polar DMSO but further work will be needed to understand this observation.

4. Conclusions

Scheme 2 represents the most plausible and inclusive mechanism that describes this system. We have shown that the kinetics of bromide dissociation from $[Cu^{I}(PMDETA)Br]$ to form the activating catalyst $[Cu^{I}(PMDETA)(MeCN)]^+$ are rate limiting in MeCN and not the subsequent atom transfer activation reaction. The kinetics of this ligand exchange reaction were determined to be ~3 orders of magnitude slower in MeCN in comparison with DMSO. The fact that activation is much faster in DMSO overall is due to the much greater concentration of $[Cu^{II}(PMDETA)(DMSO)_2]^{2+}$ at the beginning

of the experiment due to a weaker bromide association constant for Cu(II) relative to MeCN. This is counterbalanced by a much lesser degree of bromide dissociation from Cu(I) in DMSO. We have also shown that the essential bromide dissociation reaction from the copper can be suppressed by the addition of excess free bromide which completely prevents catalysis.

Acknowledgements

We gratefully acknowledge the Australian Research Council for financial support and also assistance from Prof. Graeme Hanson with the EPR spectroscopy measurements.

5. References

1. A. Jenkins, R. Jones and G. Moad, *Pure and Applied Chemistry*, 2010, **82**, 483-491.
2. J. S. Wang and K. Matyjaszewski, *Journal of the American Chemical Society*, 1995, **117**, 5614-5615.
3. M. Kato, M. Kamigaito, M. Sawamoto and T. Higashimura, *Macromolecules*, 1995, **28**, 1721-1723.
4. W. A. Braunecker and K. Matyjaszewski, *Progress in Polymer Science*, 2007, **32**, 93-146.
5. A. J. Clark, F. De Campo, R. J. Deeth, R. P. Filik, S. Gatard, N. A. Hunt, D. Lastecoueres, G. H. Thomas, J. B. Verlhac and H. Wongtap, *Journal of the Chemical Society-Perkin Transactions 1*, 2000, 671-680.
6. A. J. Clark, C. P. Dell, J. M. Ellard, N. A. Hunt and J. P. McDonagh, *Tetrahedron Letters*, 1999, **40**, 8619-8623.
7. A. J. Clark, G. M. Battle, A. M. Heming, D. M. Haddleton and A. Bridge, *Tetrahedron Letters*, 2001, **42**, 2003-2005.
8. M. Benedetti, L. Forti, F. Ghelfi, U. M. Pagnoni and R. Ronzoni, *Tetrahedron*, 1997, **53**, 14031-14042.
9. F. Ghelfi, F. Bellesia, L. Forti, G. Ghirardini, R. Grandi, E. Libertini, M. C. Montemaggi, U. M. Pagnoni, A. Pinetti, L. De Buyck and A. F. Parsons, *Tetrahedron*, 1999, **55**, 5839-5852.
10. F. Ghelfi and A. F. Parsons, *Journal of Organic Chemistry*, 2000, **65**, 6249-6253.
11. M. Di Vaira and P. L. Orioli, *Acta Crystallographica Section B*, 1968, **24**, 595-599.
12. G. Kickelbick, T. Pintauer and K. Matyjaszewski, *New Journal of Chemistry*, 2002, **26**, 462-468.
13. B. Murphy and B. Hathaway, *Coord. Chem. Rev.*, 2003, **243**, 237-262.
14. M. Becker, F. W. Heinemann and S. Schindler, *Chemistry-a European Journal*, 1999, **5**, 3124-3129.
15. C. Würtele, O. Sander, V. Lutz, T. Waitz, F. Tuczek and S. Schindler, *J. Am. Chem. Soc.*, 2009, **131**, 7544-7545.
16. M. J. Scott and R. H. Holm, *J. Am. Chem. Soc.*, 1994, **116**, 11357-11367.
17. W. A. Braunecker, T. Pintauer, N. V. Tsarevsky, G. Kickelbick and K. Matyjaszewski, *J. Organomet. Chem.*, 2005, **690**, 916-924.
18. A. J. D. Magenau, N. C. Strandwitz, A. Gennaro and K. Matyjaszewski, *Science*, 2011, **332**, 81-84.
19. C. A. Bell, P. V. Bernhardt and M. J. Monteiro, *Journal of the American Chemical Society*, 2011, **133**, 11944-11947.
20. P. De Paoli, A. A. Isse, N. Bortolamei and A. Gennaro, *Chemical Communications*, 2011, **47**, 3580-3582.
21. M. Maeder and P. King, Jplus Consulting Pty Ltd, Perth, Western Australia, vers. 1.1 edn., 2012.
22. M. Rudolf and S. W. Feldberg, Bioanalytical System, West Lafayette, 3.03b edn., 2004.
23. R. A. Martinelli, G. R. Hanson, J. S. Thompson, B. Holmquist, J. R. Pilbrow, D. S. Auld and B. L. Vallee, *Biochemistry*, 1989, **28**, 2251-2258.
24. M. A. Halcrow, *Dalton Trans.*, 2003, 4375-4384.
25. M. J. Scott, S. C. Lee and R. H. Holm, *Inorg. Chem.*, 1994, **33**, 4651-4662.
26. T. F. Brennan, G. Davies, M. A. El-Sayed, M. F. El-Shazly, M. W. Rupich and M. Veidis, *Inorg. Chim. Acta*, 1981, **51**, 45-48.
27. G. Margraf, J. W. Bats, M. Wagner and H.-W. Lerner, *Inorg. Chim. Acta*, 2005, **358**, 1193-1203.
28. S. J. Barlow, S. J. Hill, J. E. Hocking, P. Hubberstey and W.-S. Li, *J. Chem. Soc., Dalton Trans.*, 1997, **0**, 4701-4704.
29. T. Pintauer, U. Reinöhl, M. Feth, H. Bertagnolli and K. Matyjaszewski, *European Journal of Inorganic Chemistry*, 2003, **2003**, 2082-2094.

30. N. Bortolamei, A. A. Isse, V. B. Di Marco, A. Gennaro and K. Matyjaszewski, *Macromolecules*, 2010, **43**, 9257-9267.
31. I. Caretti, B. Dervaux, F. E. Du Prez and S. Van Doorslaer, *Journal of Polymer Science Part A: Polymer Chemistry*, 2010, **48**, 1493-1501.
32. R. N. Patel, N. Singh, V. L. N. Gundla and U. K. Chauhan, *Spectrochimica Acta Part A: Molecular and Biomolecular Spectroscopy*, 2007, **66**, 726-731.
33. N. V. Tsarevsky, W. A. Braunecker and K. Matyjaszewski, *Journal of Organometallic Chemistry*, 2007, **692**, 3212-3222.
34. W. Tang, N. V. Tsarevsky and K. Matyjaszewski, *Journal of the American Chemical Society*, 2006, **128**, 1598-1604.
35. J. Kulis, C. A. Bell, A. S. Micallef and M. J. Monteiro, *Journal of Polymer Science Part a-Polymer Chemistry*, 2010, **48**, 2214-2223.
36. G. Johnston-Hall and M. J. Monteiro, *Journal of Polymer Science Part A: Polymer Chemistry*, 2008, **46**, 3155-3173.
37. N. Bortolamei, A. A. Isse, A. J. D. Magenau, A. Gennaro and K. Matyjaszewski, *Angew. Chem. Int. Ed.*, 2011, **50**, 11391-11394.
38. R. J. West and S. F. Lincoln, *Journal of the Chemical Society, Dalton Transactions*, 1974, **0**, 281-284.